

A quantitative model for linking $\text{Na}^+/\text{Ca}^{2+}$ exchange to SERCA during refilling of the sarcoplasmic reticulum to sustain $[\text{Ca}^{2+}]$ oscillations in vascular smooth muscle

Nicola Fameli Cornelis van Breemen^{†‡} Kuo-Hsing Kuo[†]

Department of Anesthesiology, Pharmacology and Therapeutics

The University of British Columbia

2176, Health Sciences Mall, Vancouver, B. C., Canada V6T 1Z3

tel 1-604-8225565; fax 1-604-8222281

[†]Contributed equally to this article.

[‡]Corresponding author. email: breemen@interchange.ubc.ca

Abstract

We have developed a quantitative model for the creation of cytoplasmic Ca^{2+} gradients near the inner surface of the plasma membrane (PM). In particular we simulated the refilling of the sarcoplasmic reticulum (SR) via PM-SR junctions during asynchronous $[\text{Ca}^{2+}]_i$ oscillations in smooth muscle cells of the rabbit *inferior vena cava*. We have combined confocal microscopy data on the $[\text{Ca}^{2+}]_i$ oscillations, force transduction data from cell contraction studies and electron microscopic images to build a basis for computational simulations that model the transport of calcium ions from $\text{Na}^+/\text{Ca}^{2+}$ exchangers (NCX) on the PM to sarcoplasmic/endoplasmic reticulum Ca^{2+} ATPase (SERCA) pumps on the SR as a three-dimensional random walk through the PM-SR junctional cytoplasmic spaces. Electron microscopic ultrastructural images of the smooth muscle cells were elaborated with software algorithms to produce a very clear and dimensionally accurate picture of the PM-SR junctions. From this study, we conclude that it is plausible and possible for enough Ca^{2+} to pass through the PM-SR junctions to replete the SR during the regenerative Ca^{2+} release, which underlies agonist induced asynchronous Ca^{2+} oscillations in vascular smooth muscle.

Keywords: Ca^{2+} oscillations, calcium signaling, vascular smooth muscle, sarcoplasmic reticulum, stochastic model.

1 INTRODUCTION

There is considerable current interest in the mechanisms whereby the intracellular messenger Ca^{2+} is able to signal different cellular functions, such as contraction, proliferation, migration and apoptosis as dictated by variable physiological stimuli or pathological insult [1]. This plasticity of Ca^{2+} signaling is dependent on the coordinated activity of the various Ca^{2+} channels, pumps and exchangers located in the PM, SR and mitochondria to generate transient or steady-state cytoplasmic Ca^{2+} gradients near Ca^{2+} -sensitive enzymes and ion channels [2]. The essence of this control system is an ultrastructural arrangement of the organelles that allows Ca^{2+} to flow from a source, e.g., a channel or $\text{Na}^+/\text{Ca}^{2+}$ exchanger (NCX) to a Ca^{2+} sink, e.g., sarcoplasmic/endoplasmic reticulum Ca^{2+} ATPase (SERCA) across a cytoplasmic microdomain with restricted diffusional characteristics, which prevent equilibration with the bulk of the cytoplasmic Ca^{2+} [3, 4, 5]. In this communication, we present a specific quantitative model for this type of linked Ca^{2+} transport, which serves to refill the SR during agonist-induced waves of SR Ca^{2+} release in vascular smooth muscle. However, it is implied that similar mechanisms may underlie the generation of different sub-cellular Ca^{2+} gradients involved in site and function specific Ca^{2+} signaling in general.

Iino and coworkers [6] discovered that activation of large arteries involved the generation and maintenance of repetitive asynchronous Ca^{2+} waves along the length of smooth muscle cells. In a subsequent series of papers, we have investigated their mechanisms in the *inferior vena cava* (IVC) of the rabbit and elucidated the following serial events (reviewed in [7]): 1) activation of IP_3 receptor channels as the first event in the signaling sequence of phenylephrine-mediated $[\text{Ca}^{2+}]_i$ oscillations leading to smooth muscle contraction; 2) activation of non-selective cation channels (NSCC; e.g., receptor- and store-operated channels, ROCs/SOCs), causing mainly influx of Na^+ into the junctional cytosol to facilitate operation of NCX in the Ca^{2+} influx mode; 3) Ca^{2+} influx through reverse NCX; 4) opening of L-type voltage gated Ca^{2+} channels (VGCCs); 5) SERCA pumping Ca^{2+} into the lumen of the junctional SR (jSR) to replenish Ca^{2+} lost during the initial release.

Our previous findings revealed that the bulk of Ca^{2+} reloading of the SR during these repetitive Ca^{2+} waves is mediated by the reversal of the NCX linked to Ca^{2+} uptake into the SR by SERCA. We postulated that this process required junctional complexes of closely

apposed PM and SR membranes separated by a narrow space characterized by restricted diffusion of calcium ions. In support of the requirement of PM-SR junctions for the maintenance of Ca^{2+} oscillations was the disappearance of the latter upon experimental separation of the two membranes [8]. However, general acceptance of the functional linkage between NCX and SERCA requires, besides experimental evidence, a quantitative demonstration that efficient, linked Ca^{2+} transport between reverse NCX in the PM and SERCA in the apposing SR is indeed plausible. We therefore carefully re-examined the ultrastructural characteristics of the PM-SR junctions in the rabbit IVC by electron microscopy, estimated from the literature what the magnitude of the junctional fluxes would have to be in order to fulfill their function of stimulating contraction and applied these geometric and dynamic parameters to a mathematical model based on random walk simulations. The close correlation between the computed fluxes and experimental data led to the conclusion that PM-SR junctional Ca^{2+} transport could function efficiently to refill the SR to maintain excitatory Ca^{2+} waves in vascular smooth muscle.

2 METHODS

2.1 Tissue preparation

All the experiments and procedures were carried out in accordance with the guidelines of the University of British Columbia Animal Care Committee (protocol number: A990290). Detailed methods have been previously described for this preparation in references [7] and [9]. Male New Zealand White rabbits (1.5–2.5 kg, obtained from Animal Care, University of British Columbia) were sacrificed by CO_2 asphyxiation and then exsanguinated. The IVC was removed, cleaned of surrounding connective tissue and then inverted. The endothelium was removed by gently wiping it with filter paper and the inverted vessel was then dissected into multiple ring segments that were 4 mm in width.

2.2 Confocal $[\text{Ca}^{2+}]_i$ measurements

The details of the confocal Ca^{2+} imaging method have been described in previous work [10]. Briefly, the inverted IVC rings were loaded with fluo-4 AM ($5 \mu\text{M}$, with $5 \mu\text{M}$ pluronic F-127) for 90 min at 25°C and then left to equilibrate for 30 minutes in normal PSS. The changes

in $[\text{Ca}^{2+}]_i$ were measured using an inverted Leica TCS SP2 AOBS, laser scanning confocal microscope with an air 10X (numerical aperture 0.3) lens. The tissue was illuminated using the 488 nm line of an Ar-Kr laser and a high-gain photomultiplier tube collected the emission at wavelengths between 505 nm and 550 nm. The acquisition rate was 3 frame/second. The measured changes in Fluo-4 fluorescence level are proportional to the relative changes in $[\text{Ca}^{2+}]_i$. All parameters (laser intensity, gain, etc.) were maintained constant during the experiment. The confocal images were further analyzed by using the Image J open source software package [11].

2.3 Electron microscopy study

Details of the electron microscopy study have been described previously [12]. Briefly, for the conventional microscopy study, the primary fixative solution contained 1.5% glutaraldehyde, 1.5% paraformaldehyde and 1% tannic acid in 0.1 M sodium cacodylate buffer that was pre-warmed to the same temperature as the experimental buffer solution (37 °C). The rings of rabbit IVC were fixed at 37 °C for 10 minutes, then dissected into small blocks, approximately 1 mm×0.5 mm×0.2 mm in size and put in the same fixative for 2 h at 4 °C on a shaker. The blocks were then washed three times in 0.1 M sodium cacodylate (30 min). In the process of secondary fixation, the blocks were post-fixed with 1% OsO₄ in 0.1 M sodium cacodylate buffer for 1 h followed by three washes with distilled water (30 min). The blocks were then further treated with 1% uranyl acetate for 1 h (*en bloc* staining) followed by three washes with distilled water. Increasing concentrations of ethanol (25, 50, 70, 80, 90 and 95%) were used (10 min each) in the process of gradient dehydration. 100% ethanol and propylene oxide were used (three 10 min washes each) for the final process of dehydration. The blocks were infiltrated in the resin (TAAB 812) and then embedded in molds and polymerized in an oven at 60 °C for 8 h. The embedded blocks were serial-sectioned on a microtome using a diamond knife at the thickness of 80 nm. The serial sections were then stained with 1% uranyl acetate and Reynolds lead citrate for 4 and 3 min, respectively. Images were obtained with a Phillips 300 electron microscope at 80 kV. The images of serial sections were further processed using Adobe Photoshop software. The PM and SR were delineated and pseudo-colored by red channel and green channel, respectively. The serial images are

further rendered and processed using the Volume J plugin in the Image J software [11].

For the immuno-electron microscopy study, in order to preserve antigenicity, the fixative was replaced with 2.5% paraformaldehyde in 0.1 M phosphate buffer saline (PBS) and post-fixation with OsO_4 was avoided. After fixation for 2 h at 4°C, the blocks were washed with 0.1 M PBS and followed with three washes with distilled water. The blocks were dehydrated with increasing concentrations of ethanol (25, 50, 60 and 70%) at 4°C. The blocks were then infiltrated and embedded in hydrophilic resin (LR white, medium hardness). The embedded blocks were sectioned and collected for immuno-labeling. The sections were incubated in 10% goat serum at 37°C for 1 h and then incubated with antibodies against NCX overnight at 4°C. After three washes of PBS, sections were labeled with secondary antibody conjugated with 10 nm colloidal gold for 2 h at 37°C. The labeled sections were stained with 1% uranyl acetate and Reynolds lead citrate for 20 and 10 min, respectively. Images were obtained with a Phillips 300 electron microscope at 60 kV.

2.4 Simulations

The computational simulations were produced by custom software code written in the C programming language on the Linux operating system [13].

Random walk simulations were implemented by using the standard pseudo-random number generator of the operating system. The pseudo-random number generator was tested separately to ensure that the degree of randomness of the generated data was adequate for our purposes.

The simulations were compiled and run on the PIII Linux cluster of the Department of Physics and Astronomy of The University of British Columbia [14].

3 RESULTS

3.1 Ca^{2+} oscillations

In the rabbit IVC-ring preparation, laser scanning confocal microscopy was applied to image subcellular Ca^{2+} waves of individual smooth muscle cells. Snap-shot images of a field of smooth muscle cells taken from the regions enclosed by two white squares, from which a set of time-series images of Ca^{2+} fluctuations was derived, are illustrated in Fig. 1A.

A representative trace of wave-like $[Ca^{2+}]_i$ oscillations in response to phenylephrine (PE) is shown in Fig. 1B. These oscillations were abolished by the application of 10 μ M KB-R7943, a NCX reverse-mode inhibitor [15]. We have previously shown that KB-R7943 is highly selective for the reverse mode of NCX in the rabbit IVC [16]. As shown in Fig. 1, KB-R7943 causes the oscillations to cease only after a finite time delay, during which the amplitude of the oscillations declines, suggestive of depletion of Ca^{2+} in the SR. In contrast, blocking the IP_3R -mediated release by administration of 2-APB, immediately abolished the $[Ca^{2+}]_i$ oscillations [16].

3.2 Ultrastructure

By the methods described in Sec. 2, we have first generated a sequential series of images from 80-nm thick slices of a smooth muscle cell. A sample image from one of the sequences is reported in Fig. 2. Sets of these images were then stacked to add depth information to the two-dimensional sections. With the use of high quality conventional electron micrographs (Fig. 2), we were able to observe the PM-SR junctional cytoplasmic space, located between the superficial SR and the apposing PM. The PM-SR junctions were often found to be associated with adjacent caveolae. The gap between the superficial SR and the apposing PM in PM-SR junctions measured approximately 20 nm. Regarding measurement of PM-SR junctions, in the present study 2 randomly selected PM-SR junctions per cell cross-section were measured from 30 different cells, corresponding to up to 60 junctions. With this unique spatial arrangement of caveolae flanking the 20 nm gap created by the superficial SR and apposing PM, the PM-SR junction forms a relatively restricted space that allows ions to accumulate to high concentrations. In order to demonstrate the three-dimensional structure of the PM-SR junction, we pseudo-colored the images and then combined the stacked serial sections and rendered them by applying a ray tracing algorithm (implemented via the Image J software package [11]) to generate pseudo-colored three-dimensional reconstructions of the PM-SR junctional regions of our sample cell. (Briefly, the ray tracing algorithm is a specific rendering algorithmic approach of three-dimensional computer graphics included in the Volume J plug-in of Image J, where mathematically modeled visualizations of programmed scenes are produced using a technique which follows rays from the eye-point outward, rather

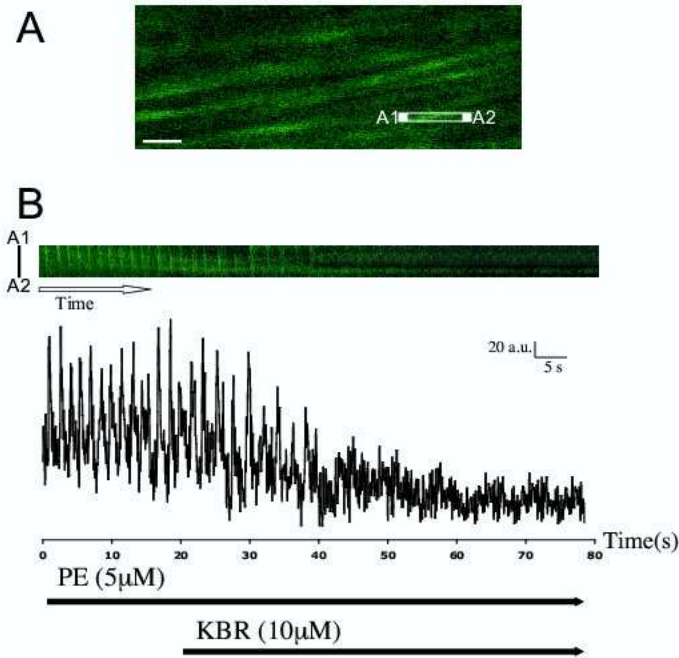


Figure 1: Phenylephrine (PE)-induced asynchronous wave-like $[Ca^{2+}]_i$ oscillations in the rabbit IVC. A: In intact rabbit IVC preparation, snap-shot images were acquired using laser scanning confocal microscopy to image subcellular Ca^{2+} waves of individual smooth muscle cells. PE ($5 \mu M$) elicited a rapid rise in $[Ca^{2+}]_i$ that appeared in the form of asynchronous Ca^{2+} waves. Ca^{2+} waves originated from distinct intracellular loci of fluorescence and traveled along the longitudinal axis of long ribbon-shaped smooth muscle cells. The region between the two white squares (A1 and A2) was selected to record the fluctuation of $[Ca^{2+}]_i$. The white scale bar in this panel corresponds to $10 \mu m$. B: The fluctuation of $[Ca^{2+}]_i$ between A1 and A2 was recorded over a time period of 80 s and plotted according to a time series. In the presence of PE, the region between A1 and A2 demonstrated fluctuations of $[Ca^{2+}]_i$ to form wave-like oscillations over time. The PE-induced Ca^{2+} waves were abolished in the presence of KB-R7943, an NCX reverse-mode inhibitor.

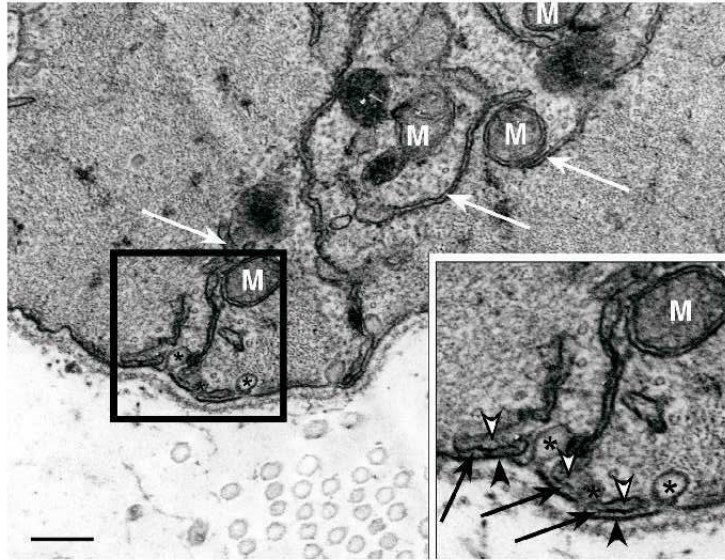


Figure 2: Representative image of serial sections of smooth muscle cell from rabbit IVC obtained by transmission electron microscopy. This is one of the serial-section images used to generate three-dimensional images of PM-SR junctional regions of vascular smooth muscle cells. The inset on the lower-right corner is a magnified image of the area enclosed by the black square. Superficial SR (indicated with white arrow heads) is observed to be apposed to PM (indicated with black arrow heads) and is flanked by two adjacent caveolae (indicated with black asterisks). In the core region of the vascular smooth muscle cell, deep SR (indicated with white arrows) can be found to be associated with mitochondria (indicated with M). In the inset, the PM-SR junction (indicated with black arrows) can be fully appreciated at high magnification. The black scale bar corresponds to 200 nm.

than originating at the light sources. It produces results similar to ray casting and scan-line rendering, but facilitates more advanced optical effects, such as accurate simulations of reflection and refraction, and is still efficient enough to be of practical use.) In Fig. 3, we present four snap shots of three-dimensional images at different angles with respect to the z-axis for every 90 degrees. The PM is visible in red, the SR in green, while white arrows indicate the PM-SR junction. In panel A, the SR is situated in a position further away from the PM so that the plasmalemmal side of the superficial SR may be observed.

In panel B, the view demonstrates the plasmalemmal side of the PM. The arrowhead indicates the opening of a caveola on the PM. The view of panel C is in a position that is rotated 180 degrees with respect to the z-axis of panel A. The image of panel C also provides a cross-sectional view of the junctional space, as indicated by the arrows. Two caveolae, as

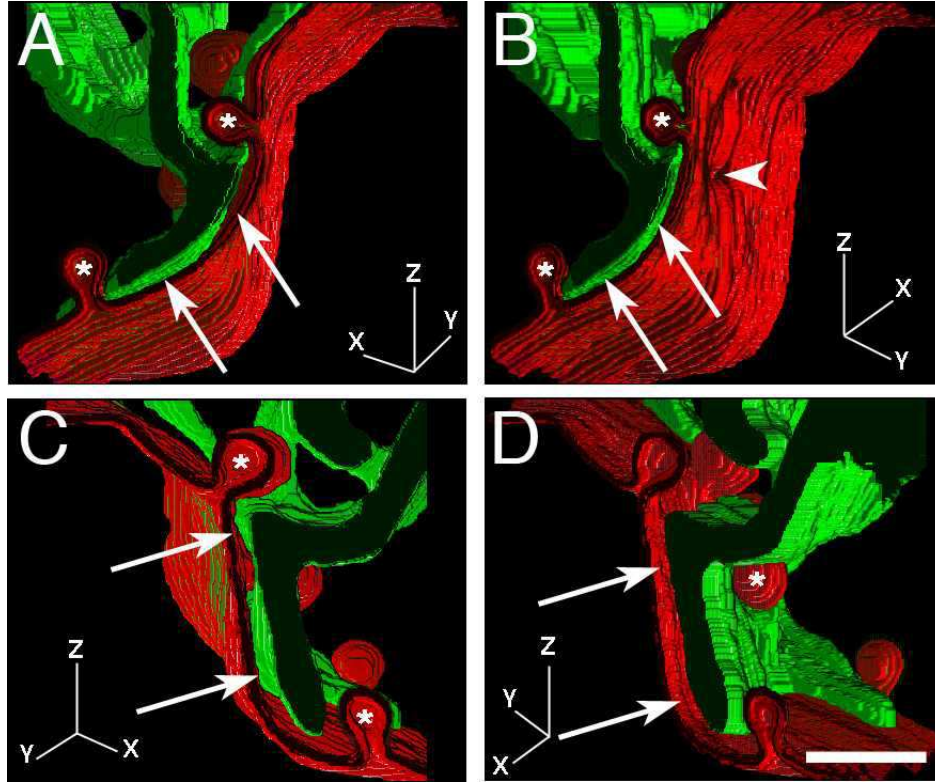


Figure 3: Pseudo-color recreation of PM-SR diffusional barrier (junctional space) regions of rabbit IVC smooth muscle cell. The PM is represented in red and the SR in green. The PM-SR junctional space regions are indicated by white arrows, and caveolae by white asterisks. The white arrowhead points to the mouth of a caveola in the PM. The white scale bar in panel D corresponds to 50 nm. The images in this figure are screenshots taken from the animation provided as online supplement to this article and they are four different views of the three-dimensional reconstruction.

indicated by the asterisks, are associated with the SR and flank the lateral opening of the junctional space. In panel D, the view is from the cytoplasmic side of the SR. The PM is situated in a position further away from the SR allowing for the cytoplasmic side of the PM and SR to be visualized as well as the protrusion of the caveolae through the superficial SR into the cytoplasmic space.

To investigate localization of the NCX transporters, the immuno-electron microscopy technique was applied to label the NCX transporters. In an effort to preserve antigenicity and increase the readability of the gold particle localization, muscle cells were processed with a milder fixative, compared to the fixatives used for the conventional electron microscopy study (as described in the Methods section). As can be noticed in Fig. 4, the use of a mild fixative inevitably compromised the preservation of cellular morphology detail; however,

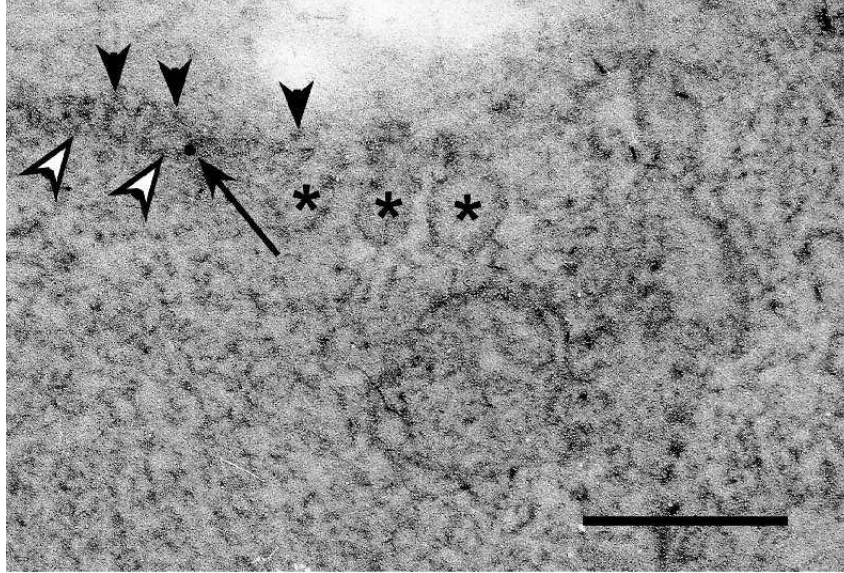


Figure 4: Immunogold labeling of NCXs: caveolae are indicated by black asterisks, the SR is indicated by white arrowheads and the PM by black arrowheads. The gold particles (identified by black arrows) are recognizable by their sharp edges. The black scale bar in this figure corresponds to 100 nm. See text for explanation of the reasons for poorer resolution of this kind of images compared to the high membrane resolution ones displayed in Fig. 2

sufficient detail was preserved to determine the localization of gold particles. We measured the surface density of gold particles in the PM to be $(100 \pm 35) \mu\text{m}^{-2}$ in regions belonging to PM-SR junctions, while it is $(4.0 \pm 1.3) \mu\text{m}^{-2}$ in regions of the PM not facing the SR.

3.3 Model foundation

Two main sets of information constitute the basis of our computational model. Firstly, a survey of the literature indicates that for each full contractile activation of a typical smooth muscle cell, the amount of Ca^{2+} supplied to the myoplasm (ΔCa^{2+}) is of the order of $100 \mu\text{mol}$ per liter of cells [3, 17, 18]. In our PM-SR junctional refilling model, this quantity is released from the SR while the SR is replenished via Ca^{2+} entry through the PM-SR junction [4]. The second information set relates to ultrastructure of the PM-SR junctions, including their incidence, typical geometrical shapes and dimensions [7]. Electron microscopy revealed that about 15% of the smooth muscle cell PM is closely apposed by the SR. Furthermore, these images suggest that the typical junction is about 20 nm in height and extends in two dimen-

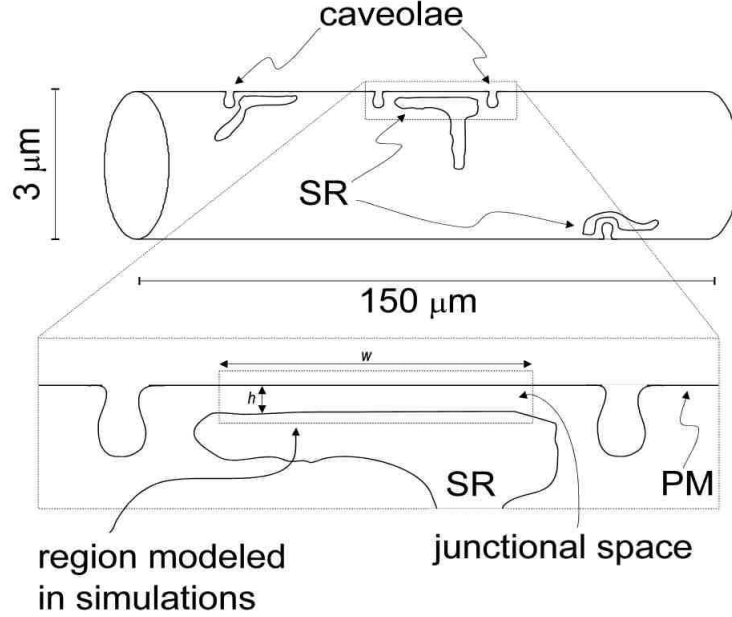


Figure 5: Diagram of smooth muscle cell and diffusional barrier regions considered in our model, where h and w are the height and width of the junction determined, on average, from ultrastructural images as 20 nm and 400 nm, respectively.

sions for about 400 nm.

The idea then is that to replenish the sarcoplasmic reticulum during the development of a full contraction, about $100 \mu\text{mol}$ of Ca^{2+} per liter of cells must enter the cell from the extracellular space (mainly through the NCX), traverse the junctional spaces, and enter the SR via the SERCA pumps on the SR surface facing the PM. This number may be regarded as an upper limit as it assumes for simplicity of the model that there is no direct recycling of Ca^{2+} between the cytoplasm and the SR.

Using the typically observed and reported sizes and shapes, we model the smooth muscle cell as a long, thin cylinder about $150 \mu\text{m}$ long and $3 \mu\text{m}$ in diameter (Fig. 5). We furthermore estimate the average number of junctions in a cell, by recalling that: 1) the fraction of PM surface facing junctional SR ($A_{\Sigma\text{JS}}$) is 15% of the smooth muscle cell surface (A_{SMC}), which from the dimensions above is approximately $1.4 \times 10^{-9} \text{m}^2$, hence $A_{\Sigma\text{JS}} = 2.1 \times 10^{-10} \text{m}^2$; 2) the surface area of the portion of PM apposing *one* typical junction is approximately $A_{\text{JS}} \simeq 1.6 \times 10^{-13} \text{m}^2$. Then, the ratio $A_{\Sigma\text{JS}}/A_{\text{JS}}$ produces an estimate of the average number of junctions per smooth muscle cell: $N_{\text{JS}} \simeq 1300$ per cell. The number of ions corresponding to

the ΔCa^{2+} of $100\ \mu\text{mol}$ per liter of cells and which is expected to traverse those roughly 1300 junctions in each cell during the occurrence of each full contraction is: $N_{\text{Ca}^{2+}} = (100\ \mu\text{mol per liter}) \times N_{\text{A}} \times V_{\text{SMC}} \simeq 6.4 \times 10^7$, where N_{A} is Avogadro's number and V_{SMC} is the volume of a smooth muscle cell in liters (about 1 pL for our chosen cell geometry). Hence, during each contractile activation, we expect about $N_{\text{Ca}^{2+}}/1300 \simeq 5 \times 10^4$ ions crossing each junction.

From this estimate coupled with Ca^{2+} oscillation data, we can also calculate the number of ions traversing a junction per unit time during contraction. Ca^{2+} wave data from studies of the rabbit IVC show that oscillations occur with a frequency of about 0.5 Hz [16], or a period T of 2 s. Furthermore, contraction force measurements conducted in parallel with $[\text{Ca}^{2+}]$ wave observations indicate that it takes around 125 oscillations to achieve full contraction (note that we have used Fig. 2B, dotted trace, in reference [16], where nifedipine is present to block voltage-gated Ca^{2+} channels). Assuming that cellular Ca^{2+} influx happens only during the second half of each oscillation period, we then estimate that there will be $5 \times 10^4 / (125 \times T/2) \simeq 400\ \text{Ca}^{2+}/\text{s}$ traversing each junction during contraction. This assumption was made in order not to underestimate the flux density as each oscillation appears to have a release phase and a refilling phase. By taking a fixed value of the Ca^{2+} flux during each half of an oscillation, we are virtually describing the Ca^{2+} flux oscillations as a square wave, or a piece-wise constant, periodic function of time. The flux value during the second half of each $[\text{Ca}^{2+}]_i$ oscillation is approximately an average value of the actual flux in the same time interval.

As anticipated in the introduction, earlier observations from this laboratory established that this Ca^{2+} flux is mainly mediated by reverse NCX [16]. Thus, another important ingredient necessary for the computational model is information on the typical number of NCX per junction. We described previously in section 3.2 that ultrastructural electron microscopic images of smooth muscle cell slices obtained with immunolabeled gold particles yield a surface density of NCX in the junctional sections of the PM of our cells. Transforming those measured densities to suit the typical dimensions of the junctions observed (extending on average 400 nm in the two dimensions parallel to the PM), we can expect 16 ± 8 NCX per junction.

Another approach to the estimation of NCX density in our cells, based on NCX turnover

rate data, lends support to this finding. Hilgemann has determined that *maximal* NCX1.1 turnover rates (V_{\max}) in cardiac cells range from 1500 s^{-1} to 5000 s^{-1} [19, 20]. It is more difficult to find reports of accurate measurements of this quantity for smooth muscle cells, where the NCX isoforms NCX1.3 and NCX1.7 are predominantly expressed [21, 22, 23]. Earlier, some experimenters have reported NCX V_{\max} values about one order of magnitude lower in bovine and porcine arteries than the values known then for cardiac cells [24, 25]. For the purposes of this discussion, we will assume that the same difference in turnover rates between cardiac and smooth muscle cell NCX applies to our system. Under the physiological conditions present during the sarcoplasmic reticulum refilling phase observed in the rabbit IVC, it is plausible to expect a Na^+ concentration ($[\text{Na}^+]$) around 20 mM, which is indeed sufficient to switch the NCX to Ca^{2+} influx mode, but just barely (we discuss this matter further in section 4). It is then likely that the exchangers will be working at a much lower turnover rate than maximal. From data on cardiac studies on the peak outward current of the NCX1.1 as a function of $[\text{Na}^+]$ [26], we estimated that the turnover rate at the conditions expected to prevail in our junction is only a few tens per second. It is then clear that 10 to 20 NCXs per junction will suffice to provide the ionic rate calculated above.

It is interesting to use the calculations above together with data on dimensions of the typical smooth muscle cell junctions to build a picture of the crowdedness of our model junction in terms of Ca^{2+} . Representing a typical junction with a parallelepiped of side 400 nm and height 20 nm (hence a volume of $3.2 \times 10^{-18} \text{ L}$) (Fig. 6), the previously calculated flux per cycle yields a junctional Ca^{2+} concentration of about $200 \mu\text{M}$, greatly exceeding the bulk $[\text{Ca}^{2+}]_i$ (the latter is typically around 100 nM [27]). Under these conditions, assuming a Ca^{2+} is a little sphere of radius equal to the atomic Bohr radius of calcium (0.2 nm), then, if each ion were the size of an apple, the next nearest ion would on average be more than three meters away. This Ca^{2+} density in the junctions is sufficiently low that we can attempt to describe their trajectories by treating ions as individual units, moving through the junction in a random walk fashion due to diffusion in the junctional cytosol.

The data used to obtain the quantities estimated in this section are summarized in Table 1.

		References
SMC diameter	$3 \mu\text{m}$	[28]
SMC length	$150 \mu\text{m}$	[28]
jPM-jSR separation	$(20 \pm 0.4) \text{ nm}$	this article
junction lateral extension	$(382 \pm 67) \text{ nm}$	this article and [7]
surface area ratio jPM/PM	15%	[7]
Ca ²⁺ release/full contraction	100 μmol per liter of cell	[3, 17, 18]
estimated Ca ²⁺ influx for contraction	400 Ca ²⁺ /s/junction	this article
frequency of [Ca ²⁺] _i oscillations	$(0.5 \pm 0.02) \text{ Hz}$	[16]
time to maximum force	250 s	[16]
Number NCX/junction	16 ± 8	this article

Table 1: Summary of data used in the model.

3.4 Computational Model

As indicated earlier, electron microscopy of immunogold labeled proteins yielded information on the density of NCX in smooth muscle cell junctions. On the other hand, information on the density of SERCA pumps on the sarcoplasmic reticulum surface side of junctional spaces is not as easily available, nor as accurate. The maximum number of pumps to distribute on the jSR of the model junction is determined using estimations of the number of pumps per cell from data in the literature and approximate measurements of the ratio between jSR and total SR obtained from our electron micrographs of IVC smooth muscle cells.

With the above information, the geometry of our numerical simulations can be set up as illustrated in Fig. 6, where the parallelepipedal shape of the model junction is arbitrarily chosen in the interest of ease of implementation in the simulations (the exact chosen shape is a box with height of 20 nm and square bases with sides of 400 nm). While on the one hand we know with a good degree of reliability that in the observed oscillations Ca²⁺ is transported (principally) from NCX on the jPM to SERCA on the jSR, on the other, the process taking the ions from sources to sinks is very complex. It includes thermal agitation, collisions with other molecules and ionic species of the junctional cytosol, interaction with jPM and jSR and buffering/unbuffering of Ca²⁺ by junctional protein structures.¹ Ionic

¹The issue of junctional Ca²⁺ buffers is by no means a trivial one and it has been the subject of extensive theoretical studies (see for example [29, 30]). To a first level of approximation, the general effect of Ca²⁺ buffers can be described by the introduction of an “effective” diffusion coefficient into the ion transport equations.

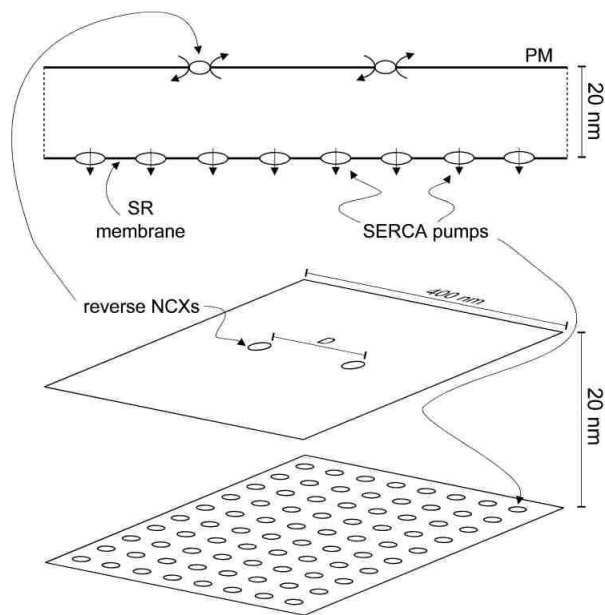


Figure 6: The model used to represent *one* junction (not to scale). The 20-nm separation between membranes and their 400-nm lateral extension are estimated from electron micrographs. The parallelepipedal shape is chosen for ease of implementation in the simulations. In them, the model junction has 2 sources on the jPM, at a distance D from each other. D varies from 0 (i.e., only one source at the center of the junctional PM (jPM)) to 400 nm (i.e., two sources at opposite edges of the jPM), while the number of sinks is left as a variable (see text for details).

trajectories under these conditions are virtually impossible to resolve deterministically by solution of the equations of motion of the individual ions. Instead, in this computational model for Ca^{2+} transport we propose that ions move around and diffuse in the junctional cytosol in a process akin to that of a gas expanding to occupy a given available volume. The term “diffuse” is used here rather loosely to encompass the set of actions causing Ca^{2+} entering the junctions via the NCX to make their way to the SERCA pumps. It is then possible to represent the ionic trajectories as a random walk in three dimensions [31, 32]. It should be emphasized that based on previous findings by this laboratory, we can exclude in this first version of the model that the activity of other transporters is of much importance to SR refilling during maintenance of the asynchronous Ca^{2+} waves studied here.

These trajectories are simulated by randomizing ionic positions starting from their entrance into the junctional space through point sources, (NCX in Fig. 6), to either their capture by a sink (SERCA in Fig. 6) or their exit from the junctional space through its

sides, which are open to the bulk cytosol. The random walk is executed on a cubic lattice of 0.2-nm steps, a value dictated by the need to compromise factors like the estimated mean free path of Ca^{2+} in the junctional cytosol, the average path length of an ion from source to sink in the junction, the values for the diffusion coefficient found in the literature (from about 10 to about 200 $\mu\text{m}^2/\text{s}$ as reported in [33]), and the need to achieve a realistic enough description of the random walk, while still keeping the simulation time reasonable. The typical distance travelled by a random walking ion and the available diffusion coefficient values yield an average travel time ranging from about 10 to about 100 μs . We have used a fixed time step value of the order of 10 ps determined from the total expected junction traversal time for a typical Ca^{2+} simulated trajectory and an average number of random walk steps taken for the traversal (the value of the diffusion coefficient D obtained as $D = (\text{space step})^2 / (6 \times \text{time step})$ is indeed of the same order of magnitude of the values found in the literature). The position of an ion, say the n -th ion, is defined by an (x_n, y_n, z_n) triad beginning from an initial position (x_n^0, y_n^0, z_n^0) coinciding with an ionic source (NCX): $(x_n^0, y_n^0, z_n^0) = (x_s, y_s, z_s)$ (where “s” stands for “source”). At each successive step ions can move with equal probability in any of the 6 directions allowed by the lattice and the new ionic position is chosen by changing the x_n , y_n , and z_n values each by 0.2 nm either positively or negatively in a random fashion, until the boundary conditions are met. In the simulations, ions encountering the jSR away from the SERCA or the jPM simply bounce off these surfaces and continue on with their random walk (perfect reflecting boundary conditions at jPM and at jSR away from the sinks). Also, ions reaching the lateral boundary of the junction are considered lost as far as the capture count is concerned (perfect absorbing conditions at lateral boundary). Sink radii are estimated at 4.5 nm from structural information on SERCA pumps obtained from the “Protein data bank” [34, 35, 36].

We can then infer the probability that ions are captured by the sinks, by taking the ratio of the number of captured Ca^{2+} over the total number of ions having entered the junction during one full contraction. The variable called “captures” in the graphs reported in Fig. 7, 8 and 9 is calculated in this way. The simulations are meant to represent a snap-shot of the captures at the end of 1 s of oscillation, i.e., the half of the oscillation corresponding to the refilling of the SR. From the Ca^{2+} influx in that phase of the oscillations estimated in the

previous section, 400 Ca^{2+} random walk through the junction and the capture probability is calculated. To obtain a ballpark figure for the uncertainty of these calculations, each datum in the graphs is the mean value from 10 repetitions of the simulations and the error bars shown correspond to 3 standard deviations from the mean.

In the proposed model, while we have an estimate of the number of sources in the junctions, we have no firm information on their position in the jPM. Moreover, there is currently very limited knowledge about the shape of the $[\text{Na}^+]_i$ gradient inside the junctional spaces. It is therefore very difficult to estimate how many of the total estimated number of junctional NCX will be active in Ca^{2+} -influx mode during each contraction-causing $[\text{Ca}^{2+}]_i$ oscillation. Because of this presently unresolved uncertainty, we have chosen to implement only two sources in our model (i. e., to consider that only two of the junctional NCX reverse) to explore two of its aspects: 1) the plausibility of the model ideas, as it is reasonable to think that if the model works with only two sources, it will work *a fortiori* with a larger number of sources; 2) the dependence of the capture rate on the relative position of the sources: the anticipated uncertainty in the details of the junctional $[\text{Na}^+]_i$ gradient and the possible proximity of some of the NCX to the edge of the junction lead us to expect that the positioning of the NCX on the jPM bear influence on the capture rate. In our computation, we have first studied the latter item by placing the sources at several distances from each other (D in Fig. 6) along an axis bisecting the jPM and calculating the capture probability under these configurations. The results are reported in Fig. 7. For this simulation we placed 100 sinks on the jSR in a regular square grid pattern (this is the way SERCA on the jSR are organized in all simulations presented here). This number is an educated guess arrived at with the benefit of hindsight via information on the turnover rates and on the reported density of SERCA pumps in SR membrane, as is explained in more detail in the next section. However, given the uncertainty in the number of pumps on the jSR, we have also calculated the capture probability *vs.* the number of sinks for our model junction. The results are shown in Fig. 8, where each set of data (indicated by different symbols and colors as described in the legend) represents the result of simulations with a different value of the inter-source distance D . The files supplied as online supplement to this article depict to-scale virtual three-dimensional views of the simulation setup, along with two typical traces of Ca^{2+} paths.

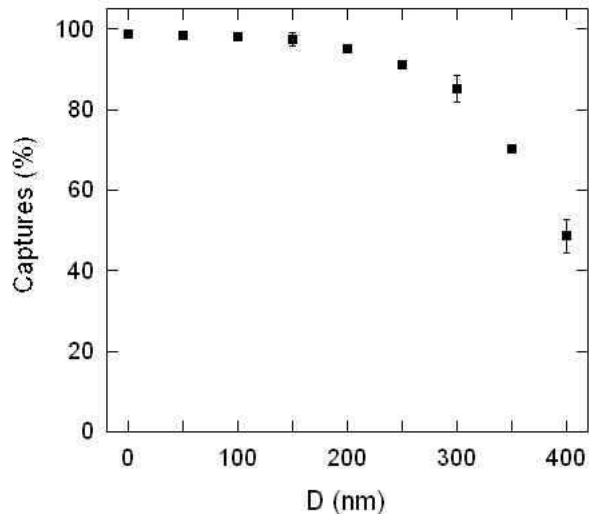


Figure 7: Results of simulations based on the model junction of Fig. 6. The “captures” are the percentage of Ca^{2+} landing on a sink (SERCA) after entering the junction from one of two sources (NCXs) and random-walking through the junction. D is the inter-source distance; a fixed number of 100 sinks was placed in the jSR for these simulations. A few representative error bars are shown. They correspond to 3 standard deviations from the mean value of 10 repetitions of the simulations at each value of D . (See online supplemental files for virtual three-dimensional view of simulation setup.)

A striking property of the PM-SR junctions is the consistency of the 20-nm width of the junctional cytoplasmic space. When this width has widened, as seen during treatment with calyculin A, the Ca^{2+} waves ceased to exist indicating that it is a critical feature for linked Ca^{2+} transport [8]. To examine this hypothesis we studied the effect on the capture rate of varying the PM-SR separation of our model junction. For this we have carried out another type of simulation, placing 2 sources in the jPM, 100 sinks in the jSR and computed the capture rate (as defined before) at different values of the jPM-jSR separation, from 0 to 400 nm. Fig. 9 illustrates the outcome of this computation, in which a random walk lattice step of 0.1 nm was used for the capture data at jPM-jSR separation values from 1 to 50 nm.

4 DISCUSSION

This work combines physiological studies on asynchronous $[\text{Ca}^{2+}]$ oscillations observed by confocal microscopy in phenylephrine-stimulated rabbit IVC and electron microscopy studies of the subcellular ultrastructure of the same cells to build a foundation for a computational

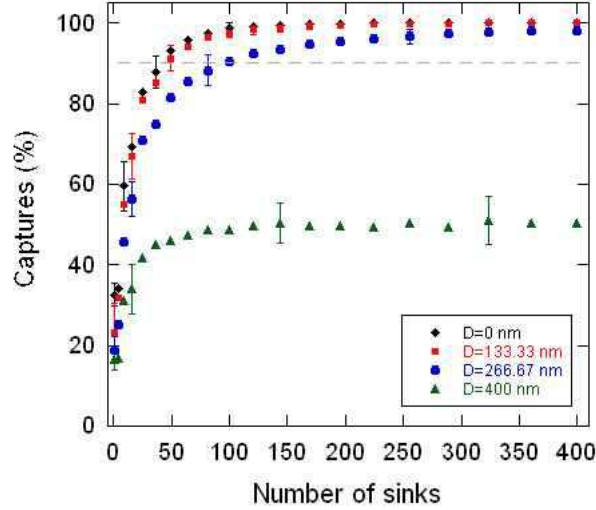


Figure 8: Results of simulations based on the model junction of Fig. 6. The “captures” are the percentage of Ca^{2+} landing on a sink (SERCA) after entering the junction from one of the two sources (NCX) and random-walking through the junction. The dashed line indicates the 90% capture rate value, which is achieved on average with about 100 sinks (except for $D = 400$ nm). Each datum in this plot is an average of 10 simulations and each set of data, indicated by the different symbols in the legend, is obtained with a different value of the inter-source distance D (Fig. 6). Error bars represent 3 standard deviations from the mean of 10 simulations. (See online supplemental files for virtual three-dimensional view of simulation setup.)

model that describes the refilling process of SR with Ca^{2+} to maintain the excitatory Ca^{2+} waves. As such it also provides a novel computational approach for simulating the cytoplasmic Ca^{2+} gradients, which are the basis for site-specific Ca^{2+} signaling in the vasculature.

The specific question we set out to address by the development of this model was whether it would be possible to move sufficient Ca^{2+} to sustain contraction through the PM-SR junctions alone, occupying only about 15% of the cell membrane surface area. Since the bulk of the refilling process is mediated by linkage of Ca^{2+} entry through reverse NCX to SERCA, we decided to model this aspect of the oscillatory Ca^{2+} cycle [16]. As such this novel approach lays the groundwork for future incorporation of other localized processes, such as NSCC mediated Na^+ influx and Na^+ extrusion by Na^+/K^+ pump $\text{NKA}\alpha_2$. The results of the numerical simulations based on the physical and physiological features of our model cells suggest that the proposed PM-SR junctional Ca^{2+} transport is indeed realistic. In spite of the scarce availability of accurate experimental data on the SERCA 2b, this pump’s

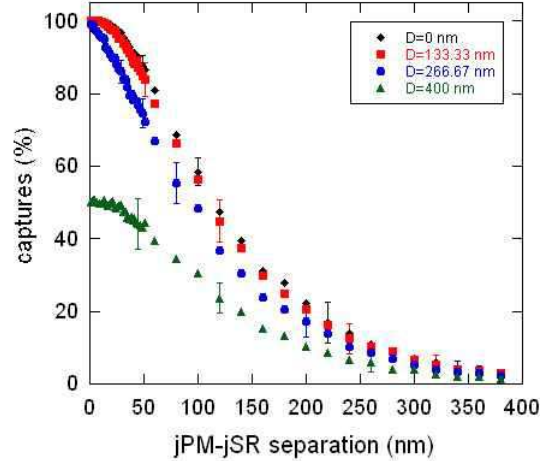


Figure 9: Results of simulations based on the model junction of Fig. 6. The capture rate is calculated at different values of the distance between the jPM and the jSR, with 100 sinks in the jSR. As in the previous graph, each datum in this plot is an average of 10 simulations and each set of data refers to a different value of the inter-source distance D (Fig. 6). The capture data for PM-SR distance values between 1 and 50 nm were obtained with a random walk lattice size of 0.1 nm.

isoform preferentially expressed in vascular smooth muscle cell, and on the NCX isoforms NCX1.3 and NCX1.7 (mainly, the maximal rates of both transporters and the density of the former are in short supply), the main simulation results reported in Fig. 8 are a strong indication that the PM-SR junctional complexes present in the smooth muscle cells of the rabbit IVC are capable of achieving the capture rates of Ca^{2+} by the SR necessary to sustain the repetitive Ca^{2+} release during excitatory $[\text{Ca}^{2+}]_i$ oscillations.

The results of Fig. 9 further highlight the possible need for the principal transporters responsible for sustaining the observed asynchronous Ca^{2+} waves to be localized in close proximity to one another by means of close apposition of the PM and the SR in junctions. The simulation data show a curvature change at a separation of 40 to 50 nm: below that value the curve appears concave downward, while it is concave upward elsewhere. This feature may be interpreted as follows. For junctional gap values below 40 to 50 nm, spillage of Ca^{2+} to the bulk cytosol is sufficiently small to guarantee efficient refilling of the SR. If instead the PM-SR separation is greater than about 40 to 50 nm, loss of Ca^{2+} from the junctional space to the bulk cytosol increases rapidly and may explain the cessation of $[\text{Ca}^{2+}]_i$ oscillations upon experimental separation of the PM from superficial SR [8].

Efficient refilling also clearly depends on the presence of an adequate number of target SERCA on the SR side of the junction. Estimates of the density of SERCA pumps in smooth muscle cells from data in the literature vary from 6 to 18 million pumps per cell [37, 38, 39]. Assuming random distribution, we can thus make a ballpark calculation of the expected number of pumps per junction by using 12 million SERCA per cell. Measurements from the ultrastructural images we present herein suggest a ratio of about 1 to 30 between jSR and total SR. Having calculated that, on average, there are 1300 junctions per cell, we arrive at an estimate of about 300 SERCA/PM-SR junction. Simulation results (Fig. 8) from our model support this figure, showing that between 200 and 400 SERCA pumps are necessary to capture more than 95% of the amount of Ca^{2+} required to refill the SR to maintain optimal smooth muscle contraction.

With respect to the NCX, its ability to reverse hinges on competition between the junctional $[\text{Ca}^{2+}]_i$ and $[\text{Na}^+]_i$. For the model to work the NCX has to reverse only at the PM-SR junctions. This requires that only there the following relation be obeyed between the electrochemical potential of Na^+ (E_{Na}), of Ca^{2+} (E_{Ca}) and the membrane potential (V_M) [40]:

$$3E_{\text{Na}} - 2E_{\text{Ca}} \leq V_M \quad (1)$$

By expanding Eq. (1), recalling that in general $E_{C^{z+}} = RT/(zF) \ln([C^{z+}]_{\text{out}}/[C^{z+}]_{\text{in}})$, where R is the universal gas constant, T the absolute temperature, C^{z+} is a z -valent cation, and F is Faraday's constant, we obtain a lower limit on the value of Na^+ concentration $[\text{Na}^+]_i$ necessary to achieve NCX reversal. We find such limit as $[\text{Na}^+]_i > 12$ mM, using $V_M = -60$ mV [41], $[\text{Na}^+]_o = 145$ mM, $[\text{Ca}^{2+}]_i = 10^{-4}$ mM, $[\text{Ca}^{2+}]_o = 1.5$ mM (ionic concentrations from [27]), $R = 8.3$ J/(mol K), $T = 310$ K, and $F = 9.65 \times 10^4$ J/(V mol). At the same time it is understood that increases in junctional $[\text{Ca}^{2+}]$ will increase the junctions $[\text{Na}^+]$ for reversal, while depolarization decreases it. Another factor favoring a higher $[\text{Na}^+]$ in the junctional space is that the low affinity isoforms $\text{NKA}\alpha_2$ and $\text{NKA}\alpha_3$, having $k_d \approx 24$ – 33 mM (k_d is the concentration of ligands at which 50% of receptors are occupied), appear to be localized at the junctions [40, 42]. The probability of NCX reversal at the junctions is further supported by measurements by our laboratory (unpublished data), which suggest a sub-plasmalemmal $[\text{Na}^+]_i$ approaching 20 mM under stimulating conditions. Using data from patch-clamp studies on Ca^{2+} influx current of cardiac sodium-calcium exchange as a

function of $[\text{Na}^+]$, we estimated that at values of $[\text{Na}^+]_i$ around 20 mM the NCX in our cell junctions would be transporting in the reverse mode at about 30% of V_{max} , or likely around 50 s^{-1} .

Clearly, it would lend considerable support to the model if the NSCC and NCX were clustered at the PM-SR junctions and if Na^+ removal was regulated not to decrease $[\text{Na}^+]_i$ below NCX reversal values. By electron microscopy of gold immunolabeled smooth muscle cells (Fig. 2 and 4), we have determined the density of NCX transporters in junctional and non-junctional regions of the PM. Our results indicate a twenty five-fold higher density of NCX in the jPM compared to the non-junctional PM. Although there is strong evidence that NSCC play a major role in the maintenance of asynchronous oscillations ([16, 43]) their possible localization at the PM-SR junctions remains to date an intriguing hypothesis. Clustering of the NSCC would give rise to non-uniform gradients that would work as position-dependent activators of Ca^{2+} -influx mode NCX.

The present quantitative model for refilling of smooth muscle SR during asynchronous $[\text{Ca}^{2+}]_i$ oscillations at the PM-SR junctions answers one important question and sets a solid stage for exploring structure and function of junctional complexes between organellar and cell membranes. The computational data presented in figures 7, 8 and 9 strongly suggest that it is possible to refill the SR through PM-SR junctional complexes, which occupy 15% of the smooth muscle cell membrane and thereby support our qualitative model derived from experimental data [7]. Some of the urgent questions related to the proposed model of PM-SR junctional Ca^{2+} transport are: 1) What are the detailed characteristics of the NCX vascular smooth muscle cell isoforms NCX1.3 and NCX1.7, specifically in regards to their V_{max} ? 2) What is the identity of the NSCC (to date it has been suggested that TRPC1 or TRPC6 are involved)? 3) Where are the NSCC localized on the PM? 4) How do the positions of NCSS, NCX, SERCA and NKA shape the junctional Na^+ and Ca^{2+} gradients to determine, together with the membrane potential, which NCX reverse? 5) What are the turnover numbers and localization of smooth muscle SERCA isoforms? 6) What is the nature of the Ca^{2+} binding sites in the junctional space and their effect on the diffusional paths of the ions? 7) Which molecules provide the glue and spacing of the cytoplasmic junctional space? In more general terms the above quantitative approach to simulating cytoplasmic Ca^{2+} domains could help

resolve important unanswered questions related to differential, time and space specific Ca^{2+} signaling of myofilament activation, mitochondrial metabolism, apoptosis, migration and differentiation.

Acknowledgments

We are indebted to Amir Ali Ahmadi for his help in the early phases of this effort. We wish to thank Andre Marziali and Jon Nakane (Applied Biophysics Laboratory, Department of Physics and Astronomy, University of British Columbia) for their invaluable input into the modeling phase of the project, as well as Damon Poburko for helpful discussions. The research was supported by grants from the Canadian Institute of Health Research and the Heart and Stroke Foundation of British Columbia and Yukon. N. F. is supported by funds from the Child and Family Research Institute (CFRI) of British Columbia. The simulations described here were performed on the “vn” cluster of the University of British Columbia (supported, in turn, by grants by the Canadian Foundation for Innovation, the British Columbia Knowledge Development Fund and the Canadian Institute for Advanced Research). We would finally like to thank the James Hogg iCapture Center for Cardiovascular and Pulmonary Research (University of British Columbia) for their support.

References

- [1] C. van Breemen, D. Poburko, E. B. Okon, TRP proteins: a new dimension in the treatment of occlusive vascular disease. *Circ. Res.* 2006;98:446–447.
- [2] M. J. Berridge, M. D. Bootman, H. L. Roderick, Calcium signalling: dynamics, homeostasis and remodelling. *Nat. Rev. Mol. Cell Biol.* 2003;4:517–529.
- [3] C. van Breemen, Calcium requirement for activation of intact aortic smooth muscle. *J. Physiol.* 1977;272:317–29.
- [4] D. Poburko, K.-H. Kuo, J. Dai, C.-H. Lee, C. van Breemen, Organellar junctions promote targeted Ca^{2+} signaling in smooth muscle: why two membranes are better than one. *Trends Pharmacol. Sci.* 2004;25:8–15.

- [5] R. Rizzuto, T. Pozzan, Microdomains of intracellular Ca^{2+} : Molecular determinants and functional consequences. *Physiol. Rev.* 2006;86:369–408.
- [6] M. Iino, H. Kasai, T. Yamazawa, Visualization of neural control of intracellular Ca^{2+} concentration in single vascular smooth muscle cells in situ. *EMBO Journal* 1994;13:5026–31.
- [7] C.-H. Lee, D. Poburko, K.-H. Kuo, C. Y. Seow, C. van Breemen, Ca^{2+} oscillations, gradients, and homeostasis in vascular smooth muscle. *Am. J. Physiol. Heart Circ. Physiol.* 2002;282:H1571–83.
- [8] C.-H. Lee, K.-H. Kuo, J. Dai, J. M. Leo, C. Y. Seow, and C. van Breemen, Calyculin-A disrupts subplasmalemmal junction and recurring Ca^{2+} waves in vascular smooth muscle. *Cell Calcium* 2005;37:9–16.
- [9] K.-H. Kuo, J. Dai, C. Y. Seow, C.-H. Lee, C. van Breemen, Relationship between asynchronous Ca^{2+} waves and force development in intact smooth muscle bundles of the porcine trachea. *Am. J. Physiol. Lung Cell. Mol. Physiol.* 2003;285:1345–53.
- [10] D. O. Ruehlmann, C.-H. Lee, D. Poburko, C. van Breemen, Asynchronous Ca^{2+} waves in intact venous smooth muscle. *Circ. Res.* 2000;86:E72–9.
- [11] Image J Version 1.33u, NIH, USA; <http://rsb.info.nih.gov/ij/>
- [12] K.-H. Kuo, L. Wang, P. D. Pare, L. E. Ford, C. Y. Seow, Myosin thick filament lability induced by mechanical strain in airway smooth muscle. *J. Appl. Physiol.* 2001;90:1811–6.
- [13] Mandrake Linux distribution, version 10.1.
- [14] <http://laplace.physics.ubc.ca/VN/>
- [15] Y. Ladilov, S. Haffner, C. Balsler-Schafer, H. Maxeiner, H. M. Piper, Cardioprotective effects of KB-R7943: a novel inhibitor of the reverse mode on $\text{Na}^+/\text{Ca}^{2+}$ exchanger. *Am. J. Physiol.* 1999;276:H1868–76.

- [16] C.-H. Lee, D. Poburko, P. Sahota, J. Sandhu, D. O. Ruehlmann, C. van Breemen, The mechanism of phenylephrine-mediated $[Ca^{2+}]_i$ oscillations underlying tonic contraction in the rabbit inferior vena cava. *J. Physiol.* 2001;534.3:641–50.
- [17] V. Y. Ganitkevich, The amount of acetylcholine mobilisable Ca^{2+} in single smooth muscle cells measured with the exogenous cytoplasmic Ca^{2+} buffer, Indo-1. *Cell Calcium* 1996;20:483–92.
- [18] B. Daub, V. Y. Ganitkevich, An estimate of rapid cytoplasmic calcium buffering in a single smooth muscle cell. *Cell Calcium* 2000;27:3–13.
- [19] D. W. Hilgemann, Unitary cardiac Na^+, Ca^{2+} exchange current magnitudes determined from channel-like noise and charge movements of ion transport. *Biophys. J.* 1996;71:759–68.
- [20] D. W. Hilgemann, New insights into the molecular and cellular workings of the cardiac Na^+/Ca^{2+} exchanger. *Am. J. Physiol. Cell Physiol.* 2004;287:1167–72.
- [21] Y. Nakasaki, T. Iwamoto, H. Hanada, T. Imagawa, M. Shigekawa, Cloning of the rat aortic smooth muscle Na^+/Ca^{2+} exchanger and tissue-specific expression of isoforms. *J. Biochem.* 1993;114:528–34.
- [22] S. L. Lee, A. S. Yu, J. Lytton, Tissue-specific expression of Na^+-Ca^{2+} exchanger isoforms. *J. Biol. Chem.* 1994;269:14849–52.
- [23] B. D. Quednau, D. A. Nicoll, K. D. Philipson, Tissue specificity and alternative splicing of the Na^+/Ca^{2+} exchanger isoforms NCX1, NCX2, and NCX3 in rat. *Am. J. Physiol. Cell Physiol.* 1997;272:C1250–61.
- [24] R. S. Slaughter, J. L. Shevell, J. P. Felix, M. L. Garcia, G. J. Kaczorowski, High levels of sodium-calcium exchange in vascular smooth muscle sarcolemmal membrane vesicles. *Biochemistry* 1989;28:3995–4002.
- [25] J. C. Docherty, T. G. Maddaford, D. F. Dubo, N. L. Choptain, G. N. Pierce, $Na(+)-Ca^{2+}$ exchange and Ca^{2+} channel characteristics in bovine aorta and coronary artery smooth muscle sarcolemmal membranes. *Mol. Cell. Biochem.* 1995;144:61–6.

- [26] D. W. Hilgemann, S. Matsuoka, G. A. Nagel, A. Collins, Steady-state and dynamic properties of cardiac sodium-calcium exchange. Sodium-dependent inactivation. *J. Gen. Physiol.* 1992;100:905–32.
- [27] B. Alberts, A. Johnson, J. Lewis, M. Raff, K. Roberts and P. Walter, *Molecular Biology of the Cell*, Garland Science, New York, U. S. A. (2002)
- [28] A. P. Somlyo, Structural characteristics, mechanisms of contraction, innervation and proliferation of smooth muscle cells. Ultrastructure and function of vascular smooth muscle. *Adv. Exp. Med. Biol.* 1975;57:1–80. Review.
- [29] J. Sneyd, Calcium buffering and diffusion: on the resolution of an outstanding problem. *Biophys. J* 1994;67:4–5.
- [30] C. P. Fall, E. S. Marland, J. M. Wagner, J. J. Tyson (Editors), *Computational Cell Biology*, New York, U. S. A. (2002)
- [31] H. C. Berg, *Random Walks in Biology*, Princeton University Press, Princeton, U. S. A. (1993)
- [32] C. A. Whitney, *Random Processes in Physical Systems: an Introduction to Probability Based Computer Simulations*, Wiley, New York, U. S. A. (1990)
- [33] N. L. Allbritton, T. Meyer and L. Stryer, Range of messenger action of calcium ion and inositol 1,4,5-triphosphate. *Science* 1992;258:1812–15.
- [34] H. M. Berman, J. Westbrook, Z. Feng, G. Gilliland, T. N. Bhat, H. Weissig, I. N. Shindyalov, P. E. Bourne, The protein data bank. *Nucleic Acid Research* 2000;28:235–42.
- [35] <http://www.pdb.org> or <http://www.rcsb.org/pdb/>
- [36] C. Toyoshima, M. Nakasako, H. Nomura, H. Ogawa, Crystal structure of the calcium pump of sarcoplasmic reticulum at 2.6 Å resolution. *Nature* 2000;405:647–55.
- [37] G. Inesi, C. Sumbilla, M. E. Kirtley, Relationships of molecular structure and function in Ca²⁺(+)-transport ATPase. *Physiol. Rev.* 1990;70:749–60.

- [38] A. B. Elmoselhi, M. Blennerhassett, S. E. Samson, A. K. Grover, Properties of the sarcoplasmic reticulum Ca(2+) pump in coronary artery skinned smooth muscle. *Mol. Cell. Biochem.* 1995;151:149–55.
- [39] M. E. Holmes, S. E. Samson, J. X. Wilson, S. J. Dixon, A. K. Grover, Ascorbate transport in pig coronary artery smooth muscle: Na(+) removal and oxidative stress increase loss of accumulated cellular ascorbate. *J. Vasc. Res.* 2000;37:390–8.
- [40] M. P. Blaustein and W. J. Lederer, Sodium/calcium exchange: its physiological implications. *Physiol. Rev.* 1999;79:763–854.
- [41] R. E. Haddock and Caryl E. Hill, Rhythmicity in arterial smooth muscle. *J. Physiol.* 2005;566:645–56.
- [42] M. Juhaszova and M. P. Blaustein, Na⁺ pump low and high ouabain affinity α subunit isoforms are differently distributed in cells. *Proc. Natl. Acad. Sci. USA* 1997;94:1800–5.
- [43] C.-H. Lee, R. Rahimian, T. Szado, J. Sandhu, D. Poburko, T. Behra, L. Chan and C. van Breemen, Sequential opening of IP₃-sensitive Ca²⁺ channels and SOC during α -adrenergic activation of rabbit vena cava. *Am. J. Physiol. Heart Circ. Physiol.* 2002;282:H1768–77.

This figure "FullBox-1.jpg" is available in "jpg" format from:

<http://arxiv.org/ps/q-bio/0603001v2>

This figure "PartBox-1.jpg" is available in "jpg" format from:

<http://arxiv.org/ps/q-bio/0603001v2>

This figure "PartBox2D-1.jpg" is available in "jpg" format from:

<http://arxiv.org/ps/q-bio/0603001v2>